Materials Letters 355 (2024) 135465

Contents lists available at ScienceDirect

Materials Letters

journal homepage: www.elsevier.com/locate/matlet

Effect of reduced graphene oxide on the structural and optical properties of ZnO nanoparticles

Ahmed I. Abdel-Salam [a], T.S. Soliman [b,c,*], A. Khalid [d,*], M.M. Awad [e], S. Abdallah [d]

[a] Nanotechnology Research Centre (NTRC), The British University in Egypt (BUE), Suez Desert Road, El Sherouk City, Cairo 11837, Egypt
[b] Physics Department, Faculty of Science, Benha University, Benha 13518, Egypt
[c] Institute of Natural Sciences and Mathematics, Ural Federal University, Ekaterinburg 620000, Russian Federation
[d] Department of Basic Engineering Sciences, Faculty of Engineering (Shoubra), Benha University, Benha, Egypt
[e] Physics Department, Loughborough University, Loughborough, Leicestershire LE11 3TU, UK

ARTICLE INFO

Keywords:
ZnO
rGO
Refractive index
UV–visible spectroscopy

ABSTRACT

The co-precipitation method was used to synthesize ZnO nanoparticles (NPs). Then, graphene oxide (GO) sheets which were reduced during the reaction process to become (rGO), were embellished with ZnO NPs. The impact of rGO on the structure and morphology of ZnO was investigated using XRD, FTIR, TEM, and SEM techniques. Investigating the optical characteristics was done using UV–vis spectroscopy. ZnO exhibits a hexagonal phase, as proved by XRD. The average crystallite size reduced from 22 to 18 nm after being anchored on rGO sheets. TEM and SEM testify to the presence of ZnO in nanoscales with quasi-spherical shapes, which dispersed homogeneously along the GO sheets. The optical bandgap was increased from 2.57 eV to 3.17 eV for ZnO and ZnO-rGO, respectively. Based on the obtained optical bandgap, the refractive index of ZnO and ZnO-rGO nanocomposite was theoretically determined using different models such as Moss and Ravindra models. ZnO-rGO nanocomposite's ability to change optical characteristics makes it a superior nominee for optoelectronic applications.

1. Introduction

Zinc oxide (ZnO) was considered one of the most important inorganic materials used in various fields of optoelectronic applications due to their numerous qualities like piezo-, -pyro-electric properties, and wide bandgap (3.1–3.3 eV) [1]. ZnO is a prominent essential material in various applications, like solar cells, photocatalysts, gas sensors, luminescent materials, coatings, and electronic components [2]. Decreasing the particle size, forming different shapes, and substitutional doping are commonly used methods to tailor the material properties, as the shape and size have the main impact on the properties of the prepared material. ZnO can be synthesized in different shapes, such as nano-rods, nano-wires, nano-belts, and nano-rings, depending on the preparation process [1,3]. Many preparation methods are used for preparation nanoparticles like sol–gel, precipitation, hydrothermal, and wet chemical methods [4]. Herein, co-precipitation method was presented to obtain pure-phase ZnO NPs. After that the obtained ZnO NPs were decorated on graphene oxide (GO) sheets to enhance their properties. Synthesis of nanocomposite based on ZnO and GO is one of the most promising and affordable strategies for tuning ZnO morphology and optical parameters [5].

Innovative thinking in the fields of communication and information technology requires consideration of optical bandgap and refractive index. Consequently, this work aimed to study the change in ZnO structure when decorated on GO sheets and their impact on the absorption and bandgap of ZnO. In addition, the refractive index is estimated using different theoretical models using the bandgap obtained from Tauc's law. ZnO and ZnO-rGO structures were investigated by XRD, SEM, TEM, and FTIR techniques. ZnO and ZnO-rGO absorption were recorded using a UV–visible spectrophotometer.

* Corresponding authors at: Physics Department, Faculty of Science, Benha University, Benha 13518, Egypt (T.S. Soliman). Department of Basic Engineering Sciences, Faculty of Engineering (Shoubra), Benha University, Benha, Egypt (A. Khalid).
E-mail addresses: tarek.attia@fsc.bu.edu.eg (T.S. Soliman), ahmed.abdelkhalik@feng.bu.edu.eg (A. Khalid).

https://doi.org/10.1016/j.matlet.2023.135465
Received 10 July 2023; Received in revised form 6 September 2023; Accepted 23 October 2023
Available online 24 October 2023

2. Experimental

2.1. Synthesis of ZnO NPs and ZnO-rGO nanocomposites

Co-precipitation was employed to produce ZnO NPs. Typically, 11gm of zinc (II) acetate dihydrate (Fisher-chemical, 99 %) was dissolved in 100 ml deionized-water and then heated to 70 °C. After that, a solution of 1 M sodium hydroxide (Merck, ≥97 %) with a volume of 100 ml was dropwise added to zinc acetate solution. The white precipitate was separated and washed with deionized-water several times using the centrifuge at 8000 rpm, then dried at 80 °C for 6hrs. Finally, the collected powder was heat treated at 400 °C for 2hrs to obtain ZnO NPs. For the ZnO-rGO nanocomposites, the GO was dispersed in Zinc (II) acetate solution, and by the same steps in ZnO preparation, the chemical reaction was completed (Fig. 1a).

2.2. Characterization

X-ray diffraction (Malvern Panalytical) was used to identify the materials' phase and crystal structure. Field-emission scanning electron microscope (Thermo-Scientific) and transmission electron microscope (Jeol JEM-2100) were used to determine nanomaterials morphology and size. SEM-EDX and EDX mapping were used to identify the elemental analysis and distribution in the samples. FT-IR spectra were recorded using Vertex-70 RAM-II, besides measuring the absorption spectra of the samples using a UV–Vis-NIR spectrophotometer.

3. Results and discussions

Fig. 1b reveals the XRD pattern of the as-prepared ZnO and ZnO-rGO nanocomposite. The peaks at 31.68°, 34.32°, 36.16°, 47.44°, 56.50°, 62.75°, and 67.86° are observed, which coincide with (1 0 0), (0 0 2), (1 0 1), (1 0 2), (1 1 0), (1 0 3) and (1 1 2) diffraction planes, respectively. These results are compatible with the hexagonal ZnO (JCPDS No. 01-079-0207).

The ZnO-rGO reveals a pattern with a slight shift in peak positions, as shown in the inset of Fig. 1b. The GO characteristic peak has not appeared due to the small quantity of GO that produces weak diffraction intensity compared with ZnO [6]. By the literature, it could result from the whole reduction of GO during ZnO growth [7]. The crystallite size was calculated using the Scherrer formula [8] and was found to be about ~ 22 and 18 nm for ZnO and ZnO-rGO nanocomposite, respectively. This is caused due to the presence of rGO, which hinders the growth of ZnO [9]. The (1 0 1) peak was shifted to a higher angle with the insertion of rGO to ZnO (inset of Fig. 1b), indicating the lessen in the d-spacing from 2.484 to 2.479 Å. Besides, the full-width at half maximum (FWHM) increases from 0.398 to 0.484, revealing a decrease in the crystalline size.

EDX analysis (Fig. 1c) of ZnO-rGO nanocomposite reveals that the sample contains Zn, O, and carbon elements. Moreover, EDX-mapping of ZnO-rGO confirms that the elemental distribution of Zn and O elements on the surface of the rGO sheets is homogeneous.

Fig. 2a shows the SEM image of ZnO with a quasi-spherical shape and particle size of about 20 nm, which was affirmed by the TEM image in Fig. 2c. When the ZnO was prepared in the presence of GO sheets, a highly porous 2D-layered structure of rGO sheets decorated with ZnO was obtained, Fig. 2b.

The ZnO supported on the rGO sheets has a particle size of about 13 nm lower than that for pristine ZnO, as shown in the TEM image in Fig. 2d. Also, it shows the attachment of ZnO on the rGO surface. The diffusion of the tiny particles of ZnO into rGO sheets during their growth is the reason for the decrease in their growth-rate and particle-size compared to the pristine ZnO. Furthermore, TEM image shows high transparency and the sheets' wrinkles of rGO sheets. This confirms the high stability of rGO sheets after the thermal-reduction process during the heat treatment of the ZnO since the sheet wrinkles prevent the re-staking of rGO sheets after the reduction process.

In Fig. 3, FT-IR spectra of GO, ZnO, and ZnO-rGO are displayed. ZnO spectrum shows characteristic bands at 430, 478, and 630 cm^{-1} related to the stretching vibration of the Zn-O bond [6]. The GO exhibited distinct bands for vibration modes of C=C, C–OH, and C–O alkoxide at 1621, 1395, and 1014 cm^{-1}, respectively [6]. Furthermore, the ZnO-rGO spectrum showed ZnO-specific bands at 430, 478, and 630 cm^{-1}, which are assigned to the Zn-O stretching vibration. In addition to the GO vibration modes at 1621 and 1414 cm^{-1}, which are assigned to the C=C and C–OH functional groups, with a slight shift in the C-OH vibration mode from 1395 to 1414 cm^{-1} indicating the binding between ZnO and rGO [8]. The peak at 1621 cm^{-1} in the GO spectrum was shifted to 1572 cm^{-1} in the ZnO-rGO spectrum, indicating the partial reduction of GO [6].

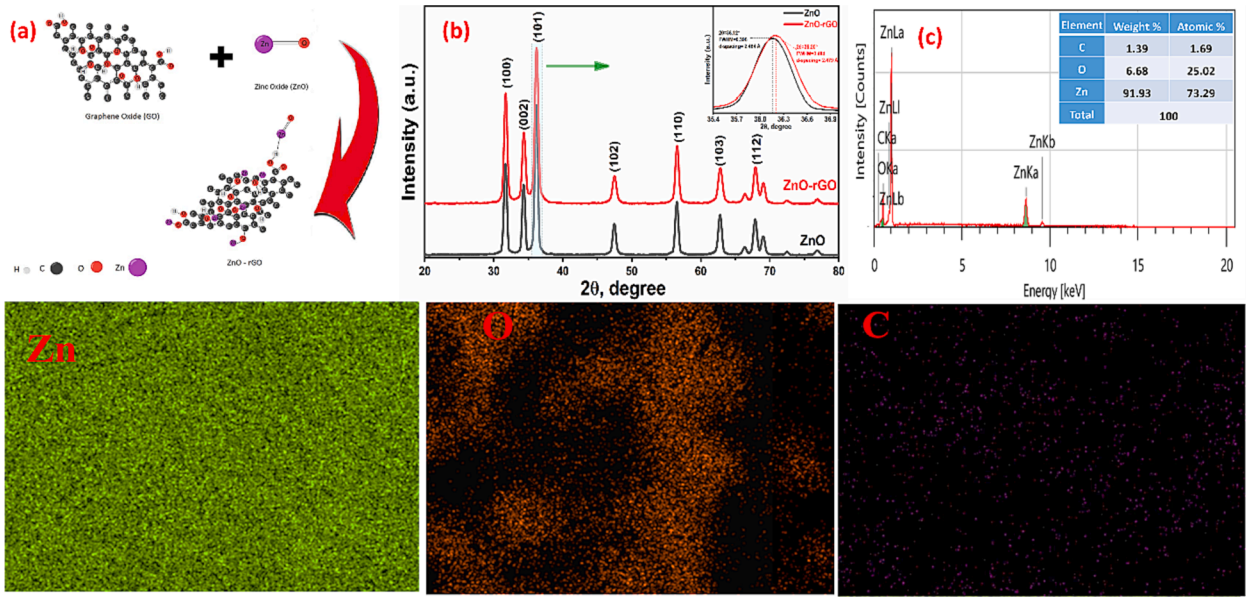

Fig. 1. (a) Synthesis of ZnO-rGO nanocomposite, (b) XRD pattern of ZnO and ZnO-rGO, and (c) EDX and elemental–mapping of Zn, O, and C for ZnO-rGO nanocomposite.

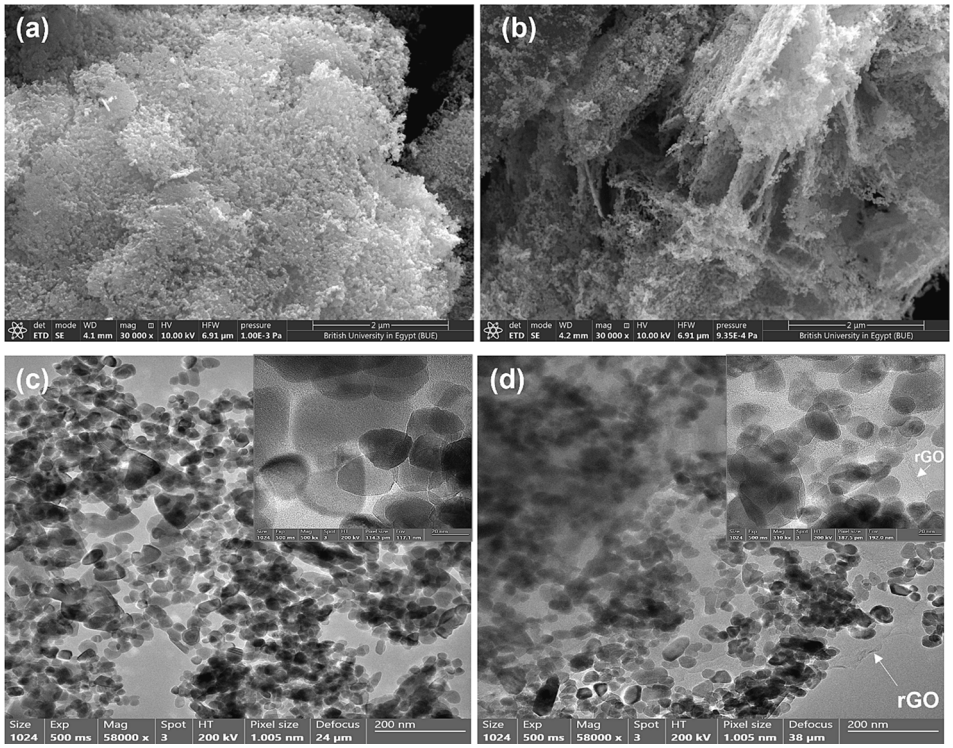

Fig. 2. SEM and TEM images of ZnO (a&c) and ZnO-rGO nanocomposites (b&d).

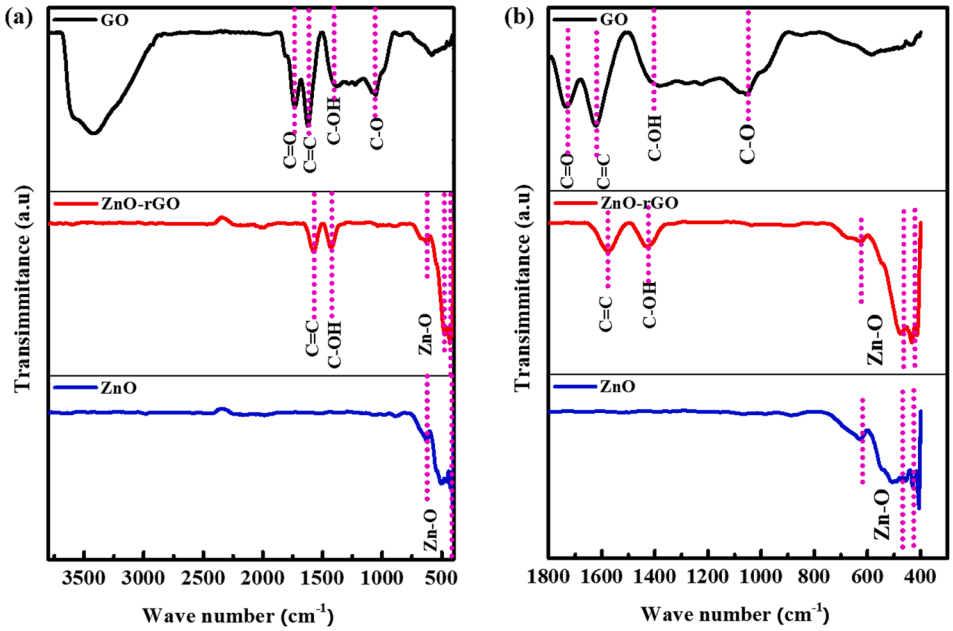

Fig. 3. FT-IR spectra of GO, ZnO, and ZnO-rGO at range (a) from 3800 to 400 cm^{-1} and (b) from 1800 to 300 cm^{-1}.

Fig. 4a shows the absorption and transmission spectra of ZnO and ZnO-rGO nanocomposites. The ZnO absorption spectrum was characterized by absorption peak at $\lambda_{max} = 380$ nm. This peak was blue shifted to lower wavelength value at $\lambda_{max} = 369$ nm when ZnO was decorated on rGO sheets.

The optical bandgap E_g was calculated using the formula, $E_g = 1240/\lambda_{max}$. The E_g values are 3.26 and 3.36 eV for ZnO and ZnO-rGO, respectively. An increase in E_g is related to the quantum confinement phenomena (as the particle size decreases, the bandgap increases) [8].

The absorption coefficient (α), the incident photon energy (hυ), and the direct bandgap related to Tauc's law (E_{gd}^{Tauc}) are correlated as follows [8];

$$(\alpha h\upsilon)^2 = constant\left(h\upsilon - E_{gd}^{Tauc}\right) \quad (1)$$

Extrapolating the linear portion of the relationship between $(\alpha h\upsilon)^2$ versus (hυ) (Fig. 4b) with the x-axis (at $h\upsilon = 0$) represents (E_{gd}^{Tauc}). The E_{gd}^{Tauc} value increases from 2.57 eV for ZnO to 3.17 eV for ZnO-rGO. The

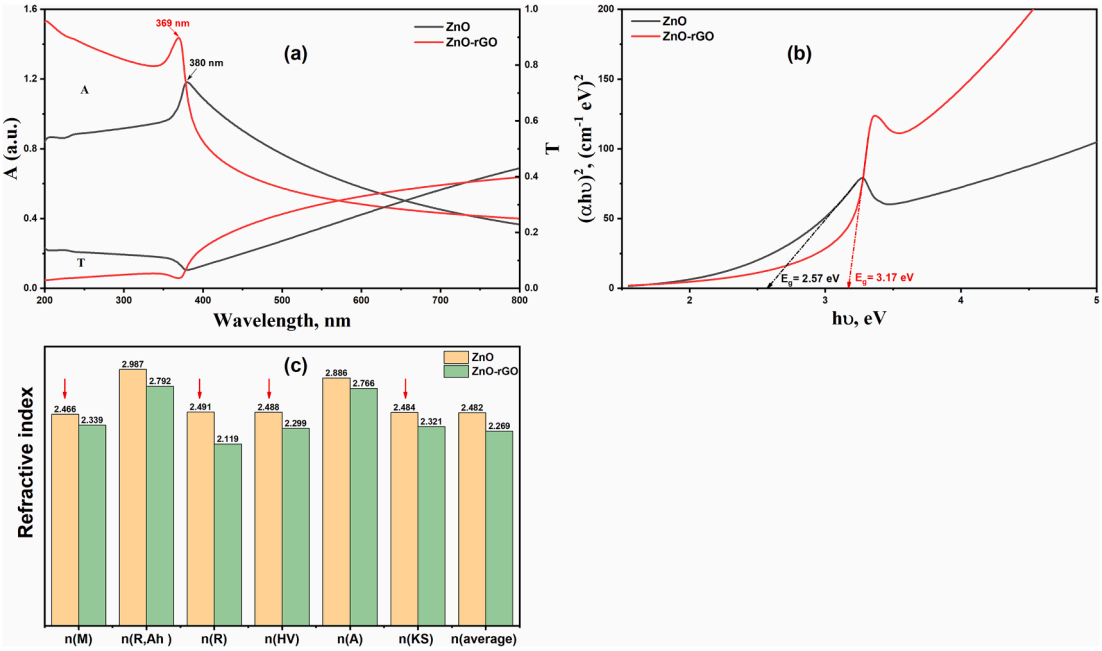

Fig. 4. (a) Absorption and transmission spectra, (b) $(\alpha h\upsilon)^2$ vs. hυ of ZnO and ZnO-rGO NPs, and (c) refractive index of ZnO and ZnO-rGO for various theoretical models.

rGO sheets hinder the ZnO particle size growth, which is approved by XRD and TEM analysis. This is compatible with the literature [9]. According to the quantum confinement effect, as the particle size decreases, the bandgap increases [10].

Many models, including moss (n_M), Reddy-Ahammed ($n_{R,Ah}$), Ravindra (n_R), Herve and Vandamme (n_{HV}), Kumar-Singh (n_{KS}), and Annani et al. (n_A), demonstrated the inverse relationship between E_g and the linear refractive index as follow [11],

$$n_M^4 \times E_g = 95eV \tag{2}$$

$$n_{R,Ah}^4 = \frac{154eV}{(E_g - 0.365eV)} \tag{3}$$

$$n_R = 4.084 - 0.62E_g \tag{4}$$

$$n_{HV} = \sqrt{1 + [\frac{13.6eV}{E_g + 3.4eV}]^2} \tag{5}$$

$$n_{KS} = 3.3668 \times E_g^{-0.32234} \tag{6}$$

$$n_A = 3.4 - 0.2E_g \tag{7}$$

The refractive indices were calculated using (E_{gd}^{Tauc}) and the data were displayed in Fig. 4c. The refractive indices are approximately coincided for all models except for Annani and Reddy-Ahammd models. The average refractive index ($n_{average}$=(n_M + n_R + n_{HV} + n_{KS})/4) was calculated regarding to the four matched models. The $n_{average}$ value is about 2.482 for ZnO which is reduced to 2.269 after decoration of ZnO NPs on the GO sheets. Due to low packing density, the material's reflectance drops, and its transparency increases as the particle size lowers [8].

4. Conclusion

ZnO nanoparticles were prepared through the co-precipitation method and successfully supported on rGO sheets. XRD confirms the synthesis of the ZnO single phase. rGO sheets hindered the ZnO growth, as verified by TEM analysis. TEM analysis confirmed the GO layers' formation. The UV–visible spectra showed a blue shift after ZnO anchored on rGO sheets. ZnO nanoparticles showed a bandgap widening when decorated on rGO sheets because of the quantum confinement effect. The calculated values of the refractive index were in good accordance with four models (Moss, Ravindra, Herve-Vandamme, and Kumar-Singh). The average refractive index value is about 2.482 for ZnO and reduced to 2.269 for ZnO-rGO.

CRediT authorship contribution statement

Ahmed I. Abdel-Salam: Investigation, Formal analysis, Methodology, Data curation, Writing – original draft. **T.S. Soliman:** Conceptualization, Formal analysis, Investigation, Methodology, Data curation, Writing – review & editing. **A. Khalid:** Conceptualization, Formal analysis, Investigation, Methodology, Data curation, Writing – review & editing. **M.M. Awad:** Investigation, Formal analysis, Writing – original draft. **S. Abdallah:** Conceptualization, Formal analysis, Methodology, Writing – review & editing.

Declaration of Competing Interest

The authors declare that they have no known competing financial interests or personal relationships that could have appeared to influence the work reported in this paper.

Data availability

No data was used for the research described in the article.

References

[1] K. Davis, R. Yarbrough, M. Froeschle, J. White, H. Rathnayake, RSC Adv. 9 (2019) 14638–14648.
[2] N. Kamarulzaman, M.F. Kasim, R. Rusdi, Nanoscale Res. Lett. 10 (2015) 1–12.
[3] I. Boukhoubza, I. Derkaoui, M.A. Basyooni, M. Achehboune, M. Khenfouch, W. Belaid, M. Enculescu, E. Matei, Mater. Chem. Phys. 306 (2023), 128063.
[4] Y.H. Ni, X.W. Wei, J.M. Hong, Y. Ye, Mater. Sci. Eng. B Solid-State Mater. Adv. Technol. 121 (2005) 42–47.
[5] I. Boukhoubza, M. Khenfouch, M. Achehboune, L. Leontie, A.C. Galca, M. Enculescu, A. Carlescu, M. Guerboub, B.M. Mothudi, A. Jorio, I. Zorkani, Nanomaterials 10 (2020) 1–16.
[6] K. Kacem, S. Ameur, J. Casanova-Chafer, M.F. Nsib, E. Llobet, J. Mater. Sci. Mater. Electron. 33 (2022) 16099–16112.
[7] R. Lv, X. Wang, W. Lv, Y. Xu, Y. Ge, H. He, G. Li, X. Wu, X. Li, Q. Li, J. Chem. Technol. Biotechnol. 90 (2015) 550–558.
[8] A.I. Abdel-Salam, M.M. Awad, T.S. Soliman, A. Khalid, J. Alloy. Compd. 898 (2022), 162946.
[9] I. Boukhoubza, M. Khenfouch, M. Achehboune, L. Leontie, A. Carlescu, J. Alloy. Compd. 831 (2020), 154874.
[10] W. Alamgir, S. Khan, M.M. Ahmad, A.H.N. Hassan, Opt. Mater. (Amst.) 38 (2014) 278–285.
[11] R.M. Ahmed, T.S. Soliman, S.A. Vshivkov, A. Khalid, Physica Scripta 98 (2023), 055928.